Giant Optical Manipulation

Vladlen G. Shvedov,[1,2,3] Andrei V. Rode,[1] Yana V. Izdebskaya,[2,3] Anton S. Desyatnikov,[2]
Wieslaw Krolikowski,[1] and Yuri S. Kivshar[2]

[1]*Laser Physics Center, Research School of Physics and Engineering, Australian National University, Canberra ACT 0200, Australia*
[2]*Nonlinear Physics Center, Research School of Physics and Engineering, Australian National University, Canberra ACT 0200, Australia*
[3]*Department of Physics, Taurida National University, Simferopol 95007, Ukraine*

(Received 22 July 2010; revised manuscript received 13 August 2010; published 10 September 2010)

We demonstrate a new principle of optical trapping and manipulation increasing more than 1000 times the manipulation distance by harnessing strong thermal forces while suppressing their stochastic nature with optical vortex beams. Our approach expands optical manipulation of particles into a gas media and provides a full control over trapped particles, including the optical transport and pinpoint positioning of ~ 100 μm objects over a meter-scale distance with ± 10 μm accuracy.

DOI: 10.1103/PhysRevLett.105.118103 PACS numbers: 87.80.Cc, 37.10.Mn, 37.10.Pq

Introduction.—Since its discovery 40 years ago, the ability to remotely control and move objects in space by the radiation pressure of light provides a useful tool for manipulating microscopic particles [1–3], living cells [4], nanoparticles [5], and atoms [6,7], and is increasingly employed in biology and physics [3,8]. However, the operation of weak radiation pressure forces, such as a gradient force in optical tweezers [2,4] and a scattering force in optomechanics [9], is restricted to small spatial scale, typically hundreds of microns. In contrast, thermal or radiometric forces can be much stronger [10], and they may extend a spatial scale of all-optical manipulation [11]. However, radiometric forces dominate for light-absorbing particles interacting with surrounding media, and thus far their stochastic nature prevent stable large-scale trapping of particles and aerosols [3,12].

When a surface of an aerosol particle is heated nonuniformly by light, the surrounding gas molecules rebound off the surface with different velocities creating an integrated force on the particle. This effect was discovered by Ehrenhaft [13] and is known as *photophoresis* [10,14]. A rough comparison [15] of the radiation pressure force exerted by a beam with power P, $F_a = P/c$, and the photophoretic force for particles with zero thermal conductivity, $F_{\mathrm{pp}} = P/3\nu$ [16], shows that for air at room temperature the latter dominates by several orders of magnitude, $F_{\mathrm{pp}}/F_a = c/3\nu \cong 6 \times 10^5$, where c is the speed of light, and ν is the molecular velocity.

A possibility to trap micron-sized particles in a vortex beam by employing thermal photophoretic forces was demonstrated in our recent studies [11,17] of millimeter-long optical guiding of light-absorbing aerosols with a pair of counter-propagating doughnutlike vortex beams. These earlier experiments [11] paved a road to a novel idea of utilizing the photophoretic force [18] for a reliable large-scale transport of trapped particles. In this Letter we demonstrate, for the first time to our knowledge, that the optical-to-mechanical energy conversion due to photophoretic forces can be specially tailored to trap and transport macroparticles in air by using a slowly diverging vortex beam. We achieve a stable transport of ~ 100 μm particles over the meter-scale distance, which is more than 1000 times larger than the scale of any previously reported optical manipulation technique. Our approach is based on the use of a doughnutlike vortex beam [see Fig. 1] which allows us to hold light-absorbing particles in the center of the beam while minimizing the effect of stochastic nature of the thermal forces. We derived theoretical dependence of the particles speed on the vortex beam parameters, the particle size and thermal conductivity, and viscosity of the gaseous media. The experimental study of the relation between the particle velocity and its size is also presented.

Optical vortex pipeline.—We realize a giant optical manipulation using a new class of extended optical traps

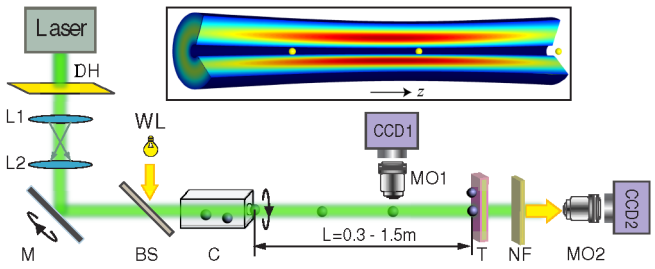

FIG. 1 (color online). Experimental setup of an optical trapping system for long-range transport of aerosol particles. The vortex beam is formed by the diffraction hologram DH; $L1$ and $L2$ are collimators which control the beam parameters, and the propagation direction is controlled by the moving mirror M. Particle transport visualization is performed in the longitudinal (microscope MO1) and transverse (microscope MO2) directions; BS—beam splitter; T—glass target; NF—notch filter to cut off the laser radiation;WL—white light source; and C—cuvette with particles. The inset shows the intensity distribution inside the vortex-induced pipeline. It varies from low [dark grey (blue)] to high [grey (red)] values. The arrow shows the direction z of the particles' transport, the latter are represented by (yellow) balls.

with optical vortex core. We term such trap the "optical vortex pipeline" because the bright ring of light intensity acts as a repelling "pipe wall" on particles trapped in the dark region on axis, while the axial component of thermal force pushes particles along the pipeline [see inset in Fig. 1]. The length of the vortex pipeline as well as the trapping area depend on the light intensity distribution, $I(r, z) = \{|l|^{|l|+1} r^{2|l|} \exp[-|l|r^2/w(z)^2]\}/[|l|!\pi w(z)^{2(|l|+1)}]P$ and are limited by the divergence of the beam due to diffraction. Here $w(z) = w_0\sqrt{[1 + z^2\lambda^2 l^2/(4\pi^2 w_0^4)]}$ is the vortex ring radius, $w_0 = w(0)$ is beam waist parameter, r is the radial coordinate, z is longitudinal distance from the beam waist, λ is the wavelength of light, and $l = \pm 1, \pm 2, \ldots$ is the topological charge. Our apparatus, shown schematically in Fig. 1, uses a linearly polarized vortex beam with topological charge $l = 1$ generated from a cw laser of wavelength $\lambda = 532$ nm by a single fork-type amplitude diffraction hologram (DH). A collimated low-diverging beam is formed and controlled by lens $L1 = 500$ mm and variable lens $L2 = 125$–200 mm. By adjusting the focal length of the lens $L2$ the beam waist is varied between 150 and 620 μm. The movable mirror M controlled the direction of the beam propagation for aiming transported particles on the remote target T. The beam splitter (BS), a white light source (WL), and a notch filter (NF) are used for visualization of the particle transport in the pipeline. The particles are placed in a rotating glass cuvette (C) aligned coaxially with the vortex beam at the left end of the optical pipeline. Rotating the cylinder or tapping on it caused the particles to suspend in air. Crossing the laser beam path leads to the particles being trapped on the vortex axis and subsequently transferred through the optical duct inside the optical pipeline formed by the vortex ring. The particle transport is monitored by a CCD1 camera [see Fig. 1]. The size of the transported particles, both carbon agglomerates and coated glass shells, is varied from 20 to 120 μm, with the mass from subnanograms up to 50 ng. The maximum laser power inside the trap is 1.5 W. Experiments on the targeted remote deposition in Fig. 4 are performed by aiming the vortex beam with mirror M to a desired position on a glass plate T and transporting a particle to this position.

Trapped particles.—In our proof-of-principle experiments, we use two types of particles to demonstrate giant optical manipulation in air. Both have high absorption of laser light and very low bulk density. The first type of particles [see Fig. 2] are agglomerates of carbon nanoparticles of 3 to 6 nm in diameter with complex internal structure [19] produced by high-repetition-rate laser ablation of graphite targets. This carbon nanofoam presents a substance closest to the ideal black body, and thus it serves as a suitable reference object for the studies of optical transport of light-absorbing particles in air [11,17,20] owing to its low bulk density of the order of 0.01 g/cm^3 and low thermal conductivity and extremely low reflectivity, $\sim 2 \times 10^{-6}$. The irregular shape of carbon nanofoam agglomerates, however, present considerable challenges for controlled manipulation as well as quantitative studies [19,21].

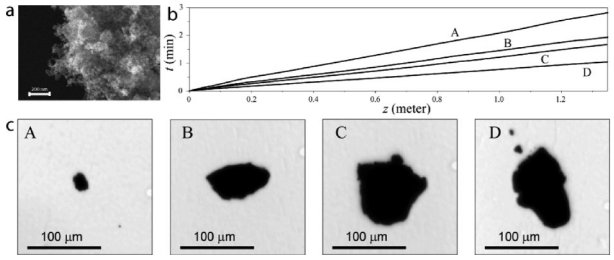

FIG. 2. Carbon particles used for the giant transport and manipulation. (a) Structure of trapped carbon particles by scanning electron microscopy. (b) Measured time of flight t for four different particles in the 1.5 m-long optical vortex pipeline. The average photophoretic speed $\langle v \rangle$ and its variation during transport is $\langle v^2 \rangle = 8.1 \pm 0.4$ mm/s for the particle marked (A), 11.7 ± 0.6 mm/s (B), 13.7 ± 0.7 mm/s (C), and 21.8 ± 0.7 mm/s (D). (c) Optical microscope images of particles deposited on the substrate after the measurements in (b).

The second type of particles are hollow glass microspheres coated with a carbon layer to increase light absorption [see Fig. 3]. Spherical microshells were prepared using commercially available microshells (3M^{TM} Scotchlite^{TM} Glass Bubbles $K1$) with typical bulk density of 0.125 g/cm^3 and thermal conductivity ~ 0.047 W m^{-1} K^{-1}. The size distribution varies from few microns to 150 μm, with average diameter 65 μm (50% by volume). The microsphere wall thicknesses are evaluated by measuring the walls of broken shells under the electron microscope; their typical thickness varied between 0.4 and 0.8 μm [see Figs. 3(a)–3(c)]. The typical depth of coating layer of carbon is in the range of 150 to 200 nm. The advantage of using microspheres is the elimination of random body-fixed thermal forces as well as a more accurate evaluation of their mass: a typical mass of a 100 μm shell is of order of 10^{-8} g. The glass microspheres also serve as a model for a transport container, which could be filled with gases, ultrapure materials, or biological substances.

Photophoretic velocity.—The ideal spherical shape and high surface quality of the shells should allow for a higher degree of control and repeatability of measurements. Figure 3(f) shows the dependence of average photophoretic velocity on the shell size measured in a 30 cm-long section of the pipeline. As it was shown in [11,17] both, longitudinal (F_z) and transfer (F_R) components of thermal force inside the vortex core [radius $w(z)$] acting upon a particle with radius a ($a \leq w$) can be expressed as $F_z \cong \kappa a^4 P/(2w^4)$ and $F_R \cong -4\kappa a^3 RP/(3w^4)$, R is a distance of the particle from the vortex center, κ is the photophoretic efficiency [17]. Photophoretic velocity [10] is defined as the stationary velocity $\vec{v}$ reached by moving spherical particle of radius a, under the action of constant photo-

phoretic force $\vec{F}_z$, and in equilibrium with the viscous drag of the medium, $\vec{F}_z + \vec{S} = 0$, here $\vec{S} = -6\pi\mu a\vec{v}$ is the Stokes' drag force and μ is the medium viscosity; $\mu = 1.73 \times 10^{-5}$ N s m^{-2} for air at room temperature. As can be seen in Fig. 1, the profile of a vortex beam changes considerably along the trap because of diffraction spreading; thus, the photophoretic force $\vec{F}_z(z)$ dependence [17] on propagation distance z cannot be neglected. It follows that, in general, the transport speed in the vortex pipeline, $v = |\vec{v}|$, depends on the particle's axial position z. This dependence is usually small in our experiments with the variation of speed comparable with measurement's accuracy; thus, speed variation cannot be reliably resolved. Therefore, we adopt the following procedure to estimate characteristic photophoretic speed from the measurements of the particles' time of flight, $t(z)$ depicted in Fig. 2(b) and 3(f). For a randomly chosen interval (z_1, z_2) within optical vortex pipeline of the length L, $0 \le z_1 \le z \le z_2 \le L$, we estimate the average speed, $v_n = (z_2 - z_1)/[t(z_2) - t(z_1)]$; here index n is the number of random realization, $n = 1, \ldots, N$. The average photophoretic speed $\langle v \rangle$ and its variation in the pipeline are then calculated as the mean and standard deviation of the vector $\vec{v}_n$, and the convergence is usually achieved for $N > 100$. Strictly speaking, the average on the interval $(0, L)$ is equivalent to the ratio of the mean square speed, $\langle v^2 \rangle$, to the average speed, $\bar{v} = L/[t(L) - t(0)]$, i.e., $L^{-1}\int_0^L v dz = \langle v^2 \rangle/\bar{v}$. We neglect the difference, $\langle v \rangle \cong \langle v^2 \rangle/\bar{v}$, because the averaging on the same z intervals allows us to compare different particles moving in the same "effective potential" produced by the vortex beam variation, as well as estimate the corresponding variation of the photophoretic speed together with measurement errors [see error bars in Fig. 3(f)]. Furthermore, here we assume the regime of adiabatic following, i.e., photophoretic speed varies along the beam as $v = F_z(z)/6\pi\mu a$, here $F_z = |\vec{F}_z|$. Our averaging approach allows us to recover the dependence of photophoretic speed on particle size [22],

$$\langle v \rangle \cong L^{-1}\int_0^L v dz = \int_0^L \frac{F(z)}{6\pi\mu a}\frac{dz}{L} = v_0\left(\frac{a}{w_0}\right)^3, \quad (1)$$

where

$$v_0 = \frac{\kappa P}{12\pi\mu w_0 L}\int_0^L \frac{dz}{(1 + z^2/z_0^2)^2}. \quad (2)$$

This function is used in Fig. 3(f) for numerical least-squares fit (solid curve) of experimental data with a fitting parameter v_0.

We compare the experimental data with our theoretical estimate, which predicts a cubic growth of the velocity with particle radius. Although the growth of velocity with particle size is evident, the deviation of experimental data from the fitting curve in Fig. 3(f) is significant (see dashed curves). We believe that the internal structure of particles (and associated variation in mass) explains wide margins of measured photophoretic speed in Fig. 3(f).

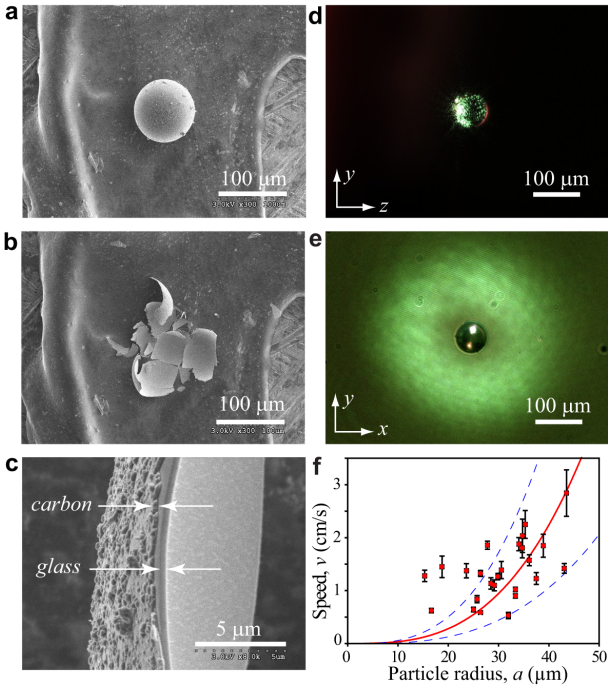

FIG. 3 (color online). Hollow glass microspheres used in giant trap experiments. (a)–(c) Scanning electron microscopy images of trapped single microsphere; (b) same sphere broken to measure shell thickness; (c) magnified edge of the broken shell showing the carbon coating layer ~180 nm and the glass shell thickness ~400 nm. (d),(e) The snapshots in longitudinal and transverse cross sections, respectively, of the particle with characteristic size $a = 35$ μm, moving in the vortex pipeline; the vortex ring radius in (d),(e) is $w = 125$ μm. (f) Average speed $\langle v \rangle$ (markers) of microspheres versus particle radius a in the optical pipeline of length $L = 30$ cm, with vortex beam waist $w_0 = 75$ μm and power $P = 0.8$ W. Solid curve: least-squares fit to experimental data, $\langle v \rangle = v_0(a/w_0)^3$, with $v_0 = 14.8 \pm 1.3$ cm/s; for comparison, dashed curves show the same function with parameter $v_0 = 27$ and 7 cm/s.

High-accuracy manipulation.—The ability of absorbing particles to be guided along the vortex core in a stable and controlled manner can be employed further for high-accuracy manipulation of particles in three dimensions. Figure 4(a) shows a schematic of controlled guidance of particles by the optical vortex pipeline and their remote targeted deposition. The control over the particle path is achieved by tilting the vortex beam with the entrance mirror located at the distance of 0.5 m away from the target [see experimental scheme in Figs. 1 and 4(a)]. The accuracy of positioning is largely determined by the laser beam pointing stability, and we could reliably pinpoint each particle within ± 10 μm from the target point in the transverse plane on the substrate—the equivalent angular accuracy of delivery is $\pm 2 \times 10^{-5}$ [Figs. 4(b) and 4(c)]. Furthermore, by varying the beam diameter we can select the size of transported and deposited particles [11], because the latter is limited from above by the vortex beam waist. Such a targeted calibration can be seen in the letter

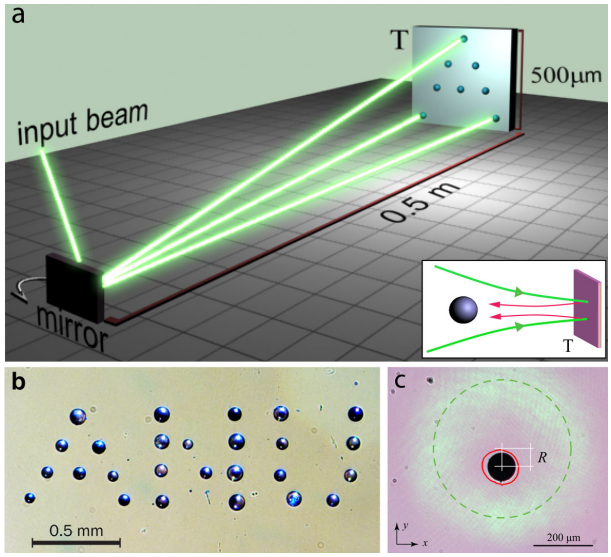

FIG. 4 (color online). Remote manipulation of particles using the optical vortex pipeline. (a) Principle of operation for targeted delivery of particles. Inset explains the method of stopping the particle before the target T using balance of forces between the main beam [light grey (green) arrows] and the beam reflected from the substrate [grey (red) arrows]. (b) Example of the remote deposition of glass microspheres; the letters "ANU" stands for the Australian National University, and the positioning accuracy is ± 10 μm over the distance of 0.5 m. (c) Transverse stability of static trapping; solid (red) line encircles the area of particle localization; the radius of the sphere $a = 50$ μm. Dashed (green) line shows the vortex ring (intensity maximum) with radius $w = 236$ μm; white lines show the transverse displacement of the particle $R = 61$ μm from vortex axis due to gravitation.

"A" in Fig. 4(b), where the diameter of deposited shell varies from 60 μm (bottom) to 100 μm (top) by varying the waist diameter from 150 μm to 250 μm.

The giant optical manipulation technique would not be complete without the possibility of a three-dimensional dynamic control of particles in real time, in addition to targeted giant transport in Fig. 4. The remote transverse manipulation of particles in air was achieved by using low-reflecting glass plate (reflectivity 7%) as a target [see the inset in Fig. 4(a)]. The converging and reflected parts of the same beam illuminate the particle from the opposite sides and create a stable three-dimensional trap, causing the particle to stop before reaching the plate T and allowing the particle to move in the transverse plane by tilting the beam with mirror M. We demonstrate such steering, and show transverse motion of a particle remotely controlled by the mirror located 0.5 m away from the particle [23].

The manipulations of absorbing particles over large distances with laser beams open up diverse practical applications. Specifically, it can be applied for touch-free transport of containers (vesicles) holding gases, ultrapure or dangerous substances, viruses, or living cells. The dual beam optical pipeline, in particular, allows us to move such a container in opposite directions, accelerate it up to several centimeters per second, or to stop and hold it anywhere in the pipeline, as we demonstrate in experiments. The method is well suited to a wide range of light-absorbing materials and ambient gases or liquids, and thus it can be applied in experimental studies of various airborne [12,24] or colloidal [4,25] particles, including atmospheric aerosols [26], as well as in experimental modeling of dusty plasmas [27] and interstellar dust [28].

This work was supported by the National Health and Medical Research Council of Australia and the Australian Research Council.

[1] A. Ashkin, Phys. Rev. Lett. **24**, 156 (1970).
[2] A. Ashkin *et al.*, Opt. Lett. **11**, 288 (1986).
[3] D. McGloin and J. P. Reid, Opt. Photonics News **21**, 20 (2010).
[4] K. Dholakia, P. Reece, and M. Gu, Chem. Soc. Rev. **37**, 42 (2008).
[5] M. Dienerowitz, M. Mazilu, and K. Dholakia, J. Nanophoton. **2**, 021875 (2008).
[6] T. Hansch and A. Schawlow, Opt. Commun. **13**, 68 (1975).
[7] S. Chu, Rev. Mod. Phys. **70**, 685 (1998).
[8] K. Svoboda and D. M. Block, Annu. Rev. Biophys. Biomol. Struct. **23**, 247 (1994).
[9] T. J. Kippenberg and K. J. Vahala, Science **321**, 1172 (2008).
[10] E. J. Davis and G. Schweiger, *The Airborne Microparticle: Its Physics, Chemistry, Optics, and Transport Phenomena* (Springer, Heidelberg 2002), pp. 780–785.
[11] V. G. Shvedov *et al.*, Opt. Express **17**, 5743 (2009).
[12] J. B. Wills, K. J. Knox, and J. P. Reid, Chem. Phys. Lett. **481**, 153 (2009).
[13] F. Ehrenhaft, Phys. Z. **18**, 352 (1917).
[14] O. Preining, in: *Aerosol Sciences*, edited by C. N. Davies (Academic Press, New York, 1966), pp. 111–135.
[15] M. Lewittes, S. Arnold, and G. Oster, Appl. Phys. Lett. **40**, 455 (1982).
[16] G. Wurm and O. Krauss, Phys. Rev. Lett. **96**, 134301 (2006).
[17] A. S. Desyatnikov *et al.*, Opt. Express **17**, 8201 (2009).
[18] M. H. Rosen and C. Orr, J. Colloid Sci. **19**, 50 (1964).
[19] A. V. Rode, E. G. Gamaly, and B. Luther-Davies, Appl. Phys. A **70**, 135 (2000).
[20] V. G. Shvedov *et al.*, Opt. Express **18**, 3137 (2010).
[21] A. V. Rode *et al.*, Appl. Phys. A **69**, S755 (1999).
[22] S. Arnold, and M. Lewittes, J. Appl. Phys. **53**, 5314 (1982).
[23] See supplementary material at http://link.aps.org/supplemental/10.1103/PhysRevLett.105.118103 for Movie 1 and Movie 2.
[24] D. McGloin *et al.*, Faraday Discuss. **137**, 335 (2008).
[25] H. Rubinsztein-Dunlop *et al.* Adv. Quantum Chem. **30**, 469 (1998).
[26] G. Wurm and O. Krauss, Atmos. Environ. **42**, 2682 (2008).
[27] A. M. Ignatov and Sh. G. Amiranashvili, Phys. Rev. E **63**, 017402 (2000).
[28] O. Krauss *et al.*, Astron. Astrophys. **462**, 977 (2007).